Dissolution kinetics of carbon in aluminum droplet combustion: Implications for aluminized solid propellants

Vincent Sarou-Kanian, Jean-Claude Rifflet, Francis Millot, Iskender Gökalp

Dissolution kinetics of carbon in aluminum droplet combustion: Implications for aluminized solid propellants

V. Sarou-Kanian[1,2,@], J.C. Rifflet[1], F. Millot[1], and I. Gökalp[2]

[1] *CNRS/CRMHT, 1D avenue de la Recherche Scientifique 45071 Orléans Cedex 2, France.*

[2] *CNRS/LCSR, 1C avenue de la Recherche Scientifique 45071 Orléans Cedex 2, France.*

[@] *to whom correspondence should be addressed (sarou@cnrs-orleans.fr).*

Full-length article

Short running title: carbon dissolution kinetics in aluminum combustion

Abstract

An analytical model describing the kinetics of carbon dissolution in burning aluminum droplets is developed in order to simulate its effects under solid rocket motors conditions. A carbon dissolution rate (k) is introduced in relation with different droplet regression laws and depending on the heterogeneous kinetics between the Al surface and the surrounding gases. The model is validated using previous experiments performed by the authors on millimeter sized Al droplets burning in several CO_2 containing atmospheres at P=1 atm. It is shown that the carbon dissolution is affected by the presence of hydrogen because of a competition between CO and H_2 chemisorptions. The model is then applied to aluminized propellants (AP/HTPB) at high pressures (P=60 atm) and high temperatures (T=3000 K and 3500 K), and considering various burning rates and adsorption conditions. Though the accuracy of the extrapolation results needs further improvements, it is shown that the carbon dissolution process should not be neglected for the global understanding of the combustion of Al particles, particularly for agglomerates.

Nomenclature

a_i = dissolution parameter

b = probability of CO adsorption/C dissolution in Al

b_0 = adsorption probability

C = carbon concentration, mol/mm^3

d = droplet diameter, mm

e_{H2} = coefficient of H_2 poisoning

E_a = activation energy, eV

k = carbon dissolution rate, mm/s

k_P = carbon dissolution rate, mm/s/atm CO

k = Boltzmann constant, 1.381×10^{-23} J/K

n = exponent of the burning d^n law

N = dissolved carbon mole number, mol

P = pressure, atm

ρ = density, mg/mm^3

S = droplet surface, mm^2

t = time, s

T = temperature, K

V = droplet volume, mm^3

Z = quantity of CO chemisorbed on Al, molecules/mm^2/s

β = burning rate, mm^n/s

Φ = carbon flux, mol/mm^2/s

Subscripts and superscripts

° = without H_2

0 = initial

Al = aluminum

b = burning

C = carbon

CO = carbon monoxide

CO2 = carbon dioxide

COX = CO and CO_2

d = droplet

H2 = dihydrogen

s = surface

sat = saturation

T = total

1 Introduction

The dissolution of carbon in aluminum droplets burning in CO_2 containing atmospheres was demonstrated in recent works [1-3]. This phenomenon is important because the amount of carbon dissolved in liquid aluminum is significant (≈ 20% mol C at P=1atm), and it has to be taken into account to understand the combustion processes particularly in aluminized solid propellants (P_{COX} up to 20 atm during the decomposition of AP/HTPB). Two main consequences of carbon dissolution on Al burning are identified. First, the increase of the carbon concentration in the droplet decreases aluminum vaporization ($P_{Al}(x_C=0.2)/P_{Al}(x_C=0)\approx 0.75$ at T=2600 K, [4,5]) and burning rates. Second, when the carbon concentration reaches its saturation limit, the excess carbon resulting from continuous droplet regression is ejected at the surface and forms a growing solid coating which also prevents Al vaporization and gas-phase burning [2] (Figure 1:Frames 1-7). A new combustion regime may therefore occur when the carbon coating interacts with the oxide cap to produce an aluminum oxycarbide phase (Figure 1:Frames 8-10). In hot ambient gases, this phase can be melted which promotes direct surface reactions. The droplet is then gradually oxidized, and dissolved carbon is finally expulsed as CO from the residue which may also be a source of fragmentation [3] (Figure 1:Frames 11-15). In fact, the carbon ejection process initiates the change of the combustion regime (gas-phase to surface reactions), but it closely depends on the preliminary dissolution conditions occurring during the first burning stage.

In the present paper, a simplified analytical model is proposed in order to describe the kinetics of carbon dissolution during the combustion of aluminum droplets. Accordingly, different droplet regression laws and heterogeneous kinetics effects are considered. The model is then

validated with the authors' experimental data, and some extrapolations for solid rocket motors conditions (particle sizes, CO_2 partial pressure, and temperature) are examined and discussed.

2 Modeling of carbon dissolution kinetics

2.1 Phenomenological approach

The analysis of such a physico-chemical problem first needs the determination of the mechanisms which may control the carbon dissolution in liquid aluminum. Obviously, the carbon dissolution results from heterogeneous kinetics between liquid Al and carbonaceous gases (CO, CO_2). However, homogenous processes, such as diffusion and chemical kinetics in gas phase, and diffusion of carbon in liquid Al, have also to be discussed.

2.1.1 Gas phase

In a combustion regime controlled by gas phase diffusion, which is typically the case of Al burning particles for low-to-moderate pressures, CO_2 is reduced by Al vapor in a diffusion flame clearly separated from the surface [1-3,6,7]. As the chemical reactions are assumed to occur with infinite kinetics, CO_2 is not present in the inner zone between the particle surface and the flame front, and only CO is the major carbonaceous species that can diffuse and react with liquid Al. In contrast, when pressure increases above 5 atm, it is suggested that the combustion regime is also controlled by chemical kinetics [7-9]. In such conditions, direct surface reactions are also possible between liquid Al and CO_2. Nevertheless, based on in King's model [10] considering finite kinetics for Al particles (d_0<50 μm) burning in CO_2/N_2 atmospheres, it is assumed that Al + CO_2 first yields to AlO + CO, and that CO then reacts with liquid Al to dissolve carbon.

2.1.2 Liquid phase

Normally, the diffusion in the liquid phase is slower than in the gas phase, and it could be assumed that the diffusion of carbon in liquid aluminum is the limitating process. However, Rossi et al. [1] showed that the carbon concentration inside quenched Al particles (d<250 μm) burning in pure CO_2 at P=1 atm was fairly homogeneous. Similarly, Sarou-Kanian et al. [2] observed that a crystallized oxycarbide phase was also homogeneously dispersed in the Al matrix for millimeter sized residues in H_2O/CO_2 mixtures. The carbon homogenization and the absence of concentration gradient in liquid aluminum, probably promoted by internal circulation (convection), suggest that the diffusion of carbon in the droplet is not controlled by diffusion in the liquid phase.

2.1.3 Liquid-gas interface

As it was previously argued for the gas phase analysis, the dissolution process first consists in the dissociative adsorption (=chemisorption) of CO (and not CO_2) on the Al surface, and then in the diffusion of atomic C in the bulk. But data about the adsorption of CO on liquid Al surface do not exist. We therefore have to refer to the general theory of heterogeneous kinetics [11] and to analogous studies [12]. In a first approximation, the adsorption process is assumed to result from translational collisions of CO molecules on the Al surface. Theoretically, the quantity of CO chemisorbed per surface unit per second (Z) on a mobile layer can be expressed as:

$$Z = b_0 \frac{P_{CO}}{(2\pi mkT)^{1/2}} e^{-E_a/kT} \quad (1)$$

with P_{CO}, m, T respectively the partial pressure, atomic mass, and temperature of CO, and b_0, E_a the probability and activation energy of adsorption of CO on liquid Al. For b_0=1 and E_a=0, we obtain the classical Hertz-Knudsen relation describing the maximum number of gas molecules

striking a surface unit in a unit time. In fact, Equation 1 shows that the adsorption process depends both on the gaseous conditions near the surface ($T \approx T_{droplet}$, P_{CO}) and on unknown adsorption parameters (b_0, E_a).

Romanowski et al. [12] has investigated the chemisorption of N_2 on liquid Al. Such work is interesting because CO and N_2 are two molecules with very close chemical structures (m=28.01 u.m.a., 3 covalent bonds, electronic ground state $^1\Sigma$, internuclear distance N_2: 1.1 Å – CO: 1.13 Å). The activation energy of the N_2 chemisorption on Al has been calculated as E_a=3.0 eV. For comparison, the dissociation energies of N_2 and CO are respectively E_{N2}=10 eV and E_{CO}=3.96 eV. This significant difference ($E_{N2}/E_{CO} \approx 2.5$) suggests that the activation energy of the CO chemisorption on Al may be lower than that of N_2; a simple rule of proportionality such as $E_a(CO) \approx E_a(N_2)/2.5$ gives a realistic estimate of the maximum activation energy for CO ($E_a \leq 1.2$ eV).

2.2 Mathematical analysis

The present model of carbon dissolution kinetics in a burning aluminum droplet is quite simple. First, the mole number of dissolved carbon at time t is considered:

$$N(t) = C(t) \cdot V(t) \tag{2}$$

with C(t) the carbon concentration (in mol C/mm^3) and $V(t) = \pi.d^3(t)/6$ the volume of the droplet at time t. Second, as the dissolution process occurs at the liquid-gas interface, N(t) can also be expressed in terms of carbon flux going inside the droplet, that is:

$$N(t) = \int_0^t \Phi(t') \cdot S(t') \cdot dt' \tag{3}$$

with $\Phi(t)$ the carbon flux (in mol C/mm^2/s) entering ($\Phi>0$) through the droplet surface $S(t) = \pi.d^2(t)$.

In order to describe this flux, the distribution of dissolved carbon in the droplet is considered homogeneous by assuming an infinitely fast diffusion of carbon in liquid aluminum (see section 2.1.2.). Accordingly, the carbon flux can be expressed as:

$$\Phi(t) = k \cdot \left(C_{sat} - C(t)\right) \tag{4}$$

with k the carbon dissolution rate (in mm/s), and C_{sat} the carbon solubility (saturation limit) in liquid Al [13]. k may be expressed such as:

$$k = \frac{b}{C_{sat}(T)} \frac{P_{CO}}{(2\pi mkT)^{1/2}} e^{-E_a/kT} \tag{5}$$

with b the probability of CO adsorption/C dissolution in liquid Al. Note that C_{sat} depends on the droplet temperature [4,5]. In fact, important parameters are P_{CO} and T. The carbon dissolution rate is directly proportional to the CO pressure, when the temperature dependence can be more or less effective according to the value of the activation energy. Indeed, for the case of E_a=0, the exponential terms are equal to unity, and the $T^{-1/2}$ term does not significantly vary at high temperatures (-20% between 2500 K and 3800 K). On the contrary, if E_a=1 eV, the adsorption can be multiplied by factor 4 for the same temperature range. This point will be discussed later especially for the extrapolation conditions.

From equations (2), (3), and (4), one can obtain:

$$N(t) = C(t) \cdot V(t) = \int_0^t k \cdot \left(C_{sat} - C(t')\right) \cdot S(t') \cdot dt' \tag{6}$$

To solve equation (9), differentiation is applied:

$$dN = C \cdot dV + V \cdot dC = k \cdot \left(C_{sat} - C\right) \cdot S \cdot dt \tag{7}$$

That is:

$$\frac{dC}{dt} = -C \cdot \left(k \cdot \frac{S}{V} + \frac{1}{V}\frac{dV}{dt} \right) + C_{sat} \cdot k \cdot \frac{S}{V} \tag{8}$$

Equation 8 is a first order differential equation with the initial condition C(t=0)=0. Its resolution depends on the expression of the droplet size evolution with time. The burning aluminum droplet size is generally considered to decrease following a "d^n law" such as $d^n(t)=d_0^n-\beta.t$ with d_0 the initial droplet diameter, and β the burning rate (in mm^n/s). n=1,1.5, and 2 are the most commonly used values. It has to be noted that β corresponds to an averaged burning rate. Indeed, it should also depend on the carbon dissolution (see Introduction).

2.2.1 Droplet size regression following a "d law": $d(t)=d_0-\beta t$

$$C(t) = C_{sat} \cdot \frac{1}{1-a_1} \cdot \left(1 - \left(1 - \frac{\beta}{d_0} \cdot t \right)^{3\left(\frac{1-a_1}{a_1}\right)} \right) \tag{9}$$

with $a_1=\beta/2k$.

2.2.2 Droplet size regression following a "d^2 law": $d^2(t)=d_0^2-\beta t$

$$\begin{aligned} C(t) = C_{sat} \cdot [\ & 1 + 3a_2 \cdot \left(1-\beta t/d_0^2\right)^{-1/2} + 6a_2^2 \cdot \left(1-\beta t/d_0^2\right)^{-1} + 6a_2^3 \cdot \left(1-\beta t/d_0^2\right)^{-3/2} \\ & - \left(1-\beta t/d_0^2\right)^{-3/2} \cdot \exp\left(\frac{\left(1-\beta t/d_0^2\right)^{1/2} - 1}{a_2} \right) \cdot \left(d_0^3 + 3a_2 \cdot d_0^2 + 6a_2^2 \cdot d_0 + 6a_2^3 \right) \ ] \end{aligned} \tag{10}$$

with $a_2=\beta/(12k\cdot d_0)$.

2.2.3 Droplet size regression following a "$d^{1.5}$ law": $d^{1.5}(t)=d_0^{1.5}-\beta t$

$$\begin{aligned} C(t) = C_{sat} \cdot \Big[& 1 + 6a_3 \cdot \left(1-\beta t / d_0^{1.5}\right)^{-1/3} + 30a_3^2 \cdot \left(1-\beta t / d_0^{1.5}\right)^{-2/3} + 120a_3^3 \cdot \left(1-\beta t / d_0^{1.5}\right)^{-1} \\ & + 360a_3^4 \cdot \left(1-\beta t / d_0^{1.5}\right)^{-4/3} + 720a_3^5 \cdot \left(1-\beta t / d_0^{1.5}\right)^{-5/3} + 720a_3^6 \cdot \left(1-\beta t / d_0^{1.5} t\right)^{-2} \\ & - \left(1-\beta t / d_0^{1.5}\right)^{-2} \cdot \exp\left(\frac{\left(1-\beta t / d_0^{1.5}\right)^{1/3} - 1}{a_3} \right) \cdot \left(d_0^3 + 6a_3 \cdot d_0^{5/2} + 30a_3^2 \cdot d_0^2 + 120a_3^3 \cdot d_0^{3/2} \right. \\ & \left. + 360a_3^4 \cdot d_0 + 720a_3^5 \cdot d_0^{1/2} + 720a_3^6 \right) \Big] \end{aligned} \tag{11}$$

with $a_3=\beta/(18k\cdot d_0^{0.5})$.

2.2.4 Droplet with no size regression, β=0, dV/dt=0

We simply obtain:

$$C(t) = C_{sat} \cdot \left(1 - e^{-\frac{6k}{d_0} \cdot t} \right) \tag{12}$$

In that case, the solubility C_{sat} occurs at $t = \infty$.

In Equations 9-11, the parameter a_i is introduced which compares the Al vaporization (β) and the carbon dissolution (k) rates. Note that it is nondimensional and depends as well on the initial particle diameter (d_0) for the "d^2 law" and the "$d^{1.5}$ law". It will be used particularly for describing the extrapolation conditions.

Figure 2 represents modeling results of carbon dissolution kinetics for an aluminum droplet of 3 mm initial diameter following a "d^2 law" (β=1.5 mm^2/s), and for several values of the carbon dissolution rate (k=0.001 to 5 mm/s). It is shown that the saturation time (t_{sat}) logically increases when the carbon dissolution rate decreases; at the lowest k, the saturation time tends to the burning time without dissolution ($t_b=d_0^2/\beta$=6 s).

3 Application of the model to Al burning experiments in CO_2 containing atmospheres

The estimation of the carbon dissolution parameters is based on Al burning experiments which were carried out previously for several CO_2 containing atmospheres (CO_2/H_2O, CO_2/H_2, CO_2/N_2, CO_2/Ar, CO_2/He, and $CO_2/H_2O/N_2$) and with different CO_2 concentrations (x_{CO2}=0.4-1), using the aerodynamic levitation technique [2,3]. For few experiments, the amount of dissolved carbon was quantified on the unburnt residues by using the technique of nuclear activation [14]. These data are particularly useful for low CO_2 concentrations because the carbon saturation is not reached when the droplet is quenched by colliding with the walls of the levitation nozzle. In that case, the experimental burning time ($t_{exp}=t_b$) may be lower than the carbon saturation time (t_{sat}). In addition, the burning experiments showing the carbon ejection at the droplet surface (Figure 1: Frame2) are also processed by assuming a carbon concentration in liquid Al equal to the saturation limit ($C(t_{exp}=t_{sat})= C_{sat}$).

Several data are needed to calculate the carbon dissolution rate. They only concern information about the Al droplet: the initial diameter (d_0), the burning or saturation time (t_b or t_{sat}), the final or saturation diameter ($d(t_b)$ or d_{sat}), the burning rate (β), and the carbon concentration ($C(t_b)$ or C_{sat}). At this step, k may be estimated (Equations 12-14) without the heterogeneous kinetics effects (T, P_{CO}). In our experiments, the varying parameter is mainly the CO_2 concentration. As expressed in Equation 5, the carbon dissolution rate is assumed proportional to the CO partial pressure, so we have introduced an intermediate parameter $k_P=k/P_{CO}$ (in mm/s/atm CO). At the surface of the burning Al droplet, P_{CO} can be expressed such as:

$$P_{CO} = \left(P_T - P_{Al,s}\right) \cdot x_{CO,f} \quad (13)$$

with P_T the total pressure (=1 atm), $P_{Al,s}$ the Al partial pressure at the droplet surface (=f(T)), and $x_{CO,f}$ the molar fraction of CO in the flame assuming stoichiometric reactions. Thus, when CO_2 is the only carbonaceous species in the oxidizing mixture, $x_{CO,f} = x_{CO2}$, and when the solid propellant conditions (AP/HTPB) are considered, the gaseous atmosphere contains both CO_2 (8-12% mol) and CO (11-20% mol), so $x_{CO,f} = x_{CO2} + x_{CO}$.

Figure 3 illustrates the simulated curves of the carbon dissolution kinetics for an aluminum burning droplet based on experimental data and for three regression size laws (d^2, $d^{1.5}$, d). k_P is adjusted in order to obtain the correct experimental burning or saturation time for the correct carbon concentration. Table 1 summarizes the k_P values estimated on 30 experiments with different CO_2 concentrations. For each experiment, k_P is quite unvarying for all the droplet regression laws. For a better analysis, the distribution of these values is shown in Figure 4. A bimodal distribution of k_P is observed with a first narrow mode located in the range [0.06-0.10], and a second wide mode in the range [0.18-0.30]. The averaged values of both modes are $k_{P1} \approx 0.08$ and $k_{P2} \approx 0.25$ mm/s/atm CO with acceptable relative errors (20% on both data, Table 2).

In fact, these modes of k_P reveal two different behaviors of the carbon dissolution kinetics which are related to the presence or the absence of hydrogenated species (H_2, H_2O) in the gaseous atmosphere. Indeed, in CO_2/(H_2O, H_2) atmospheres, k_P corresponds to the first mode ($\approx k_{P1}$), and to the second one ($\approx k_{P2}$) in pure CO_2 or CO_2/(N_2, Ar, He). Accordingly, the presence of H_2 or H_2O causes the carbon dissolution rate to decrease. This point was already discussed in [3] where it was showed that the carbon saturation time was longer in wet CO_2 than in dry CO_2 for similar droplet sizes and burning rates. First, it can be stated that it is H_2 rather than H_2O

which modifies the carbon dissolution process because H_2 is the major stable combustion product of H_2O diffusing from the flame to the droplet surface. Furthermore, the effect of H_2 results from chemical surface reactions because He which is an inert gas with close transport properties (heat and mass diffusion coefficients), does not slow down the carbon dissolution rate ($\approx k_{P2}$, see Table 1). It can be suggested that H_2 is also chemisorbed on the Al surface, and prevents partially the CO adsorption. In the theory of heterogeneous kinetics, such process is called surface poisoning [11,15] In our case, the poisoning by H_2 on the adsorption of CO on liquid Al may be expressed as:

$$k^{H2} = k^{\circ} \cdot e_{H2} \tag{14}$$

with k^{H2}, k° respectively the carbon dissolution rates with and without H_2, and e_{H2}, the parameter taking into account the hydrogen poisoning on carbon dissolution. Presently, it can be reasonably assumed that $k_P = k^{\circ} \approx 0.25$ mm/s/atm CO in dry CO_2, and $k_P \approx 0.08$ mm/s/atm CO in CO_2/(H_2O or H_2) mixtures with $e_{H2} \approx 1/3$.

4 Extrapolations to solid rocket motors

In the previous sections, the model of carbon dissolution kinetics have been applied to experiments of millimeter sized Al droplets burning in CO_2 mixtures at atmospheric pressure. This allowed estimating successfully a carbon dissolution parameter (k_P) which takes into account the CO pressure effect and the H_2 poisoning. This section aims to describe the consequences of the carbon dissolution process on the combustion of typical Al particles in solid propellant conditions, that is for submillimeter (agglomerate) and micrometer (single) sized particles in hot ambient gases at high pressures ($P_T \approx 60$ atm). Such extrapolations need to be

precautious both for the input parameters (T, P_T, $x_{CO,CO2}$), and for the significance of the results (evaluation of the uncertainties).

4.1 Input parameters

The first point which must be carefully examined is the estimation of the CO pressure at the particle surface. As expressed in Equation 16, P_{CO} is a function of the total pressure (P_T), of the Al partial pressure at the particle surface ($P_{Al,s}$), and of the molar fraction of the carbonaceous species ($x_{CO,f}$). As illustrated in Figure 5, the variation of the CO and Al vapor pressures considering solid propellant conditions (P=60 atm, $x_{CO,f}$=0.3) strongly depends on the temperature at the particle surface which is not well-known. Indeed, for classical aluminized solid propellants (AP/HTPB), the temperature of the gases in the rocket chamber at 60 atm was calculated as T=3400-3500 K (at adiabatic flame conditions, [16]). Furthermore, other works have shown that the temperature of the flame surrounding the particle varies from T=3000 K to T=3800 K for different oxidizers at P=1atm [1,6,17,18]. However, the influence of the pressure on the flame temperature is not clearly demonstrated because [7] indicated that T_{flame} was quite independent of P_{CO2} and was around 3200 K, when [19] showed that it may be higher than 4300 K at 8.6 atm in CO_2/Ar mixtures but with important uncertainties (500-1400 K). Nevertheless, further experiments performed by the latter authors [20] in similar conditions as [19], but with better optical diagnostics and analyses, measured the flame temperature in the range 3000-3200 K for P=8.5 atm in CO_2/Ar and CO_2/N_2. Therefore, because of this large temperature scattering, P_{CO} is estimated for two particle temperatures (T=3000 and 3500 K), with P_T=60 atm, and $x_{CO,f}$=0.3, that is respectively P_{CO}=17.3 and 14.3 atm.

The second point concerns the effect of temperature on the CO chemisorption. Previously, this was not taken into account to evaluate k_P (except for $P_{Al,s}$) because the droplet temperature

range in our experiments was quite narrow (2450-2600 K). For the extrapolations at higher temperatures, this effect cannot be neglected. Nevertheless, the temperature dependence also introduces the question of the activation energy (E_a). As it was shown in section 2.1.3., E_a significantly modifies the effect of temperature on the adsorption process whether it is zero or not. Thus, three activation energy values will be tested (E_a=0, 0.5, 1 eV) corresponding to the estimated energy range [0-1.2 eV].

The third point is related to the H_2 poisoning effect. As the decomposition of AP/HTPB produces significant amounts of hydrogenated species ($x_{H2O}+x_{H2}\approx0.5$), it may be reasonably assumed that this effect exists in solid propellant conditions. However, it seems difficult to estimate precisely the H_2 poisoning at higher temperatures and higher pressures. As suggested previously, the poisoning corresponds to the chemisorption of H_2 on the Al surface, which means that it also depends on adsorption parameters (P_{H2}, T, b, E_a). In section 3., it is shown that a low pressure of H_2 leads to a decrease of the carbon dissolution parameter k_P by a factor 3, but there are no information about the temperature effect; also the adsorption probability and the activation energy are unknown because they are integrated in the parameter e_{H2} (Equation 17). Accordingly, the H_2 poisoning effect will be taken into account for the extrapolations by keeping the same value for e_{H2}.

The last point concerns the carbon solubility. The Al-C (or Al-O-C) system is monovariant which means that the carbon saturation limit in liquid Al (C_{sat}) at a fixed temperature is the same for all pressures, i.e. C_{sat}=f(T). [5] have extrapolated the Al-C phase diagram for pressures up to 200 bar allowing to access C_{sat} at the three tested particle temperatures (C_{sat}(3000 K)=4.1 10^{-5}; C_{sat}(3500 K)=9.6 10^{-5} mol C/mm^3).

4.2 Intrinsic parameters

At this step, the parameter k_p (=k/P_{CO}) is no longer considered, and is replaced by the intrinsic parameter b from Equation 5 representing the probability of CO adsorption/C dissolution in liquid Al. In fact, similarly to k_P in Equation 17, b also depends on the H_2 poisoning and is expressed such as $b = b° \cdot e_{H2}$, with $b°$ the probability of adsorption/dissolution without H_2.

Table 3 summarizes the values of $b°$ and e_{H2} estimated from the experimental data with a nonlinear least squared fitting (Levenberg-Marquardt algorithm, *Origin 5.0 software*) for the three tested activation energies, considering Equation 5, and applying the "d law" and the "d² law". It is observed that, as for k_P, $b°$ is quite the same for both droplet regression laws (standard deviation ≈10%). When the activation energy increases, the probability of adsorption/dissolution also increases, and it is interesting to note that $b°$=1 corresponds E_a≈1.3 eV which is close to the qualitatively calculated maximum value (see section 2.1.3.).

With $b°$ and e_{H2}, the modeling of carbon dissolution kinetics can be then extrapolated to the propellant conditions. Table 4 and Table 5 summarize the extrapolated values of the carbon dissolution rate (k) for several conditions of temperature and adsorption (E_a) respectively considering the "d law" and the "d² law". It is observed that, for the same activation energy, k decreases when the temperature increases (k_{Max}/k_{Min}≈ 3 for 0 eV, ≈ 2.4 for 0.5 eV, ≈ 1.8 for 1 eV). In fact, this decrease of k (~Z/C_{sat}, Equation 13) mainly results from the increase of the carbon concentration limit (C_{sat}(3500 K)/C_{sat}(3000 K)≈ 2.3) compared to the lower increase of the quantity of CO chemisorbed per surface unit per second (Z(3500 K)/ Z(3000 K)≈0.9-1.6 for 0<E_a<1 eV).

4.3 Saturation diameter and saturation time

Two important data have to be extracted from such extrapolations: the saturation diameter (d_{sat}) and the saturation time (t_{sat}). Indeed, they characterize the particle size and the moment at

which the gas-phase burning ends (carbon ejection) and a second combustion regime starts. To appreciate the influence of the carbon dissolution process, d_{sat} and t_{sat} are compared respectively to the initial particle diameter (d_0) and the burning time without dissolution ($t_b=d_0^n/\beta$). Relations between d_{sat}, d_0, t_{sat}, and t_b may be easily deduced as:

$$\begin{cases} \dfrac{d_{sat}}{d_0} = 1 - \dfrac{t_{sat}}{t_b} & \text{for a "d law"} \\ \dfrac{d_{sat}}{d_0} = 1 - \left(\dfrac{t_{sat}}{t_b}\right)^2 & \text{for a "d² law"} \end{cases} \tag{15}$$

4.3.1 "d law"

The simple case concerns the carbon dissolution kinetics with the "d law". At carbon saturation, Equation 9 is simplified as:

$$\begin{cases} \dfrac{d_{sat}}{d_0} = a_1^{\frac{a_1}{3(1-a_1)}} \\ \dfrac{t_{sat}}{t_b} = 1 - a_1^{\frac{a_1}{3(1-a_1)}} \\ t_{sat} = \dfrac{\left(1 - a_1^{\frac{a_1}{3(1-a_1)}}\right)}{\beta} \cdot d_0 \end{cases} \tag{16}$$

with $a_1=\beta/2k$. These expressions are interesting because they only depend on a_1, and can be simply and rapidly applied. The third expression of Equations 20 also demonstrates the linearity between t_{sat} and d_0 which has been assumed in [3]. Figure 6 shows the evolution of d_{sat}/d_0 and t_{sat}/t_b for five orders of magnitude of a_1 values (a_1=0.01-1000), and the comparison to experimental data (a_1=0.5-5.5).

The calculation of a_1 values requires knowing the burning rate β. A review of the literature indicates that β=5-30 mm/s for $d_0 \leq 100$ µm is a realistic range [9,21,22]. The ranges of a_1 values

and their corresponding ranges of d_{sat}/d_0 and t_{sat}/t_b values are recapitulated in Table 6 (see also the dotted zone in Figure 6).

4.3.2 "d² law"

The model of carbon dissolution kinetics considering the "d² law" is more complex than that of the "d law". However, this regression law is often used for describing the combustion of aluminum particles, and the burning rate range is defined better (β=0.2-0.5 mm²/s). At the carbon saturation, Equation 10 is expressed as:

$$3a_2 \cdot \left(\frac{d_{sat}}{d_0}\right)^2 + 6a_2^2 \cdot \frac{d_{sat}}{d_0} + 6a_2^3 + \left(1 + 3a_2 + 6a_2^2 + 6a_2^3\right) \cdot \exp\left(\frac{d_{sat}/d_0 - 1}{a_2}\right) = 0 \quad (17)$$

Contrary to the model with the "d law", the resolution of Equation 17 also depends on the initial particle diameter ($a_2=\beta/(12k \cdot d_0)$). Accordingly, to extrapolate to the solid propellant conditions with this model, d_0 has to be introduced. For the *Ariane 5 MPS-230* propellant, [23] have proposed that the size distribution of the Al burning particles was globally composed of 2/3 of initial particles (≈30 µm) and 1/3 of agglomerates (≈120 µm). Table 7 recapitulates the extrapolated ranges of values of a_2, d_{sat}/d_0, and t_{sat}/t_b for the burning rate range [0.2-0.5 mm²/s] considering d_0=30 µm and d_0=120 µm. Figure 7 represents the variation of d_{sat}/d_0 and t_{sat}/t_b for 5 orders of magnitude of a_2 (0.01-1000), and the comparison to experimental data (a_2=0.1-7.33).

For both droplet regression laws, similar trends describing the evolution of a_i, d_0/d_{sat}, and t_{sat}/t_b are observed. The ranges of a_i values are wide (a_{max}/a_{min}=38 for "d law", a_{max}/a_{min}=18 for "d² law") and extend to higher values when the temperature increases. The temperature effect involves a significant shifting of the ranges of d_{sat}/d_0 and t_{sat}/t_b respectively to lower and higher

values but with a quite unvarying width of the ranges. It can also be remarked that the ranges of d_{sat}/d_0 for the "d law" are close to those for the "d^2 law" with d_0=30 µm, while the ranges of t_{sat}/t_b for the "d law" are close to those for the "d^2 law" with d=120 µm. In fact, this situation indicates that the carbon ejection process considering the "d law" occurs sooner than considering the "d^2 law" but for similar saturation diameters. Indeed, by fixing more precisely some of the input parameters, for example d_0=30 µm at T=3500 K with β_1=10 mm/s or β_2=0.3 mm²/s (same t_b=3 ms), we actually obtain d_{sat}=10-15 µm and d_{sat}=10-17 µm respectively for the "d law" and the "d^2 law" whereas t_{sat}=1.5-2 ms for the "d law" and t_{sat}=2-2.6 ms for the "d^2 law".

5 Summary and conclusions

In the present work, the carbon dissolution process during the combustion of aluminum droplets has been modeled in order to understand previous experimental results and to predict its influence in the solid rocket motors conditions. The model consists to introduce a carbon dissolution rate (k) in relation with different droplet regression laws (d, $d^{1.5}$, d^2), and depending on heterogeneous kinetics between the Al surface and the surrounding gases (CO chemisorption). Then it has been successfully applied to our own experiments of millimeter sized Al droplets burning in several CO_2 environments at atmospheric pressure (evaluation of the carbon dissolution parameter k_P), and it was shown that the carbon dissolution rate decreases in the presence of hydrogen probably because of a poisoning effect (competition between H_2 and CO chemisorptions). Based on this validation of the model, extrapolations to submillimetric and micrometric particles in hot ambient gases at high pressures have been performed by considering numerous varying parameters (particle temperature, burning rate, activation energy, H_2 poisoning). Such extrapolations allow estimating the particle size and the moment at which the carbon saturation occurs, and comparing them to the initial particle diameter and the theoretical

gas-phase burning time. The main observation concerning the extrapolation results (a_i, d_{sat}/d_0, t_{sat}/t_b) is that the carbon dissolution process cannot be neglected in the solid rocket motors conditions. Obviously, the accuracy of the results is not completely satisfactory (wide ranges of values), there are some discrepancies between the models considering the "d law" or the "d^2 law", and the variation of the particle temperature from 3000 K to 3500 K causes the shifting of the ranges of values. Nevertheless, it is shown that an Al particle detached from the propellant surface does not simply burn in a gas-phase regime until complete fuel depletion, but transforms into an intermediate residue of significant size and containing large amounts of carbon.

One important consequence of such mechanism concerns the particle size distribution of the oxide residues. As suggested in [3], carbon is not indefinitely trapped in the intermediate residues because surface reactions in hot ambient gases promote the oxidation of residual aluminum into alumina and the expulsion of carbon as CO. In this second combustion regime, it may be assumed that the size of the final residue (Al_2O_3) is close to that of the intermediate one ($Al_xO_yC_z$). Therefore, the modeling of carbon dissolution kinetics could be an interesting insight for the understanding and the prediction of oxide particle sizing.

Acknowledgments

The authors acknowledge the support of the CNRS, the Conseil Régional Centre, and the Fonds Social Européen, Objectif 2, 2000-2006.

References

1. S. Rossi, S., E.L. Dreizin, C.K. Law, Combust. Sci. and Technol., 164 (2001) 209-237.

2. V. Sarou-Kanian, J.C. Rifflet, F. Millot, E. Véron, T. Sauvage, I. Gökalp, Combust. Sci. and Technol., 177 (2005) 2299-2326.

3. V. Sarou-Kanian, J.C. Rifflet, F. Millot, I. Gökalp, Combust. Flame, 145 (2006) 220-230.

4. C. Qiu, R. Metselaar, J. Alloys and Compounds, 216 (1994) 55-60.

5. N.A. Gokcen, L.L. Oden, Ber. Bunsenges. Phys. Chem., 102:9 (1998) 1178-1180.

6. P. Bucher, R.A., Yetter, F.L. Dryer, T.P. Parr, D.M. Hanson-Parr, Proc. Combust. Inst., 27 (1996) 1899-1908.

7. B. Legrand, M. Marion, C. Chauveau, I. Gökalp, E. Shafirovich, Combust. Sci. and Technol., 165 (2001) 151-174.

8. J.C. Melcher, J.T. Brzozowski, H. Krier, R.L. Burton, AIAA paper 2000-3333 (2000).

9. J.C. Melcher, H. Krier, R.L. Burton, J. Prop. and Power, 18:3 (2002), 631-640.

10. M.K. King, Proc. Combust. Inst., 17 (1978) 1317-1328.

11. S. Gladstone, K.J. Laidler, H. Eyring, The Theory of Rate Processes, McGraw-Hill, New-York, 1941.

12. Z. Romanowski, S. Krukowski, I. Grzegory, S. Porowski, J. Chem. Phys., 114:14 (2001) 6353-6363.

13. D. Bandyopadhyay, S.D. Singh, D. Sanyal, K.K. Singh, K.N. Singh, Chem. Eng. Journ., 94 (2003) 79-92.

14. P. Goethals, C. Vandecasteele, J. Hoste, Analyt. Chim. Acta, 108 (1979) 367-370.

15. A. Clark, The Theory of Adsorption and Catalysis, Academic Press, New-York, 1970.

16. M. Marion, Etudes sur la combustion des particules d'aluminium sous pression, Thesis, Orléans University, France, 1996.

17. E.L. Dreizin, Combust. Flame, 105 (1996) 541.

18. E.L. Dreizin, Combust. Flame, 117 (1999) 841.

19. N.G. Glumac, J. Servaites, H. Krier, Combust. Sci. and Technol., 172 (2001) 97-107.

20. N.G. Glumac, H. Krier, T. Bazyn, R. Eyer, Combust. Sci. and Technol., 177 (2005) 485-511.

21. A. Davis, Combust. Flame, 7 (1963) 359.

22. Y. Shoshin, E.L. Dreizin, Combust. Flame,133 (2003) 275-287.

23. Y. Fabignon, O. Orlandi, J.F. Trubert, D. Lambert, J. Dupays, AIAA paper 2003-9731, (2003).

Tables

Table 1: Experimental data and estimated dissolution rate parameters k_P for the three "d^n laws" (n=2, 1.5, and 1). *:carbon quantification by nuclear activation; Wet: atmosphere saturated with H_2O at T=23°C.

x_{CO2}	$x_{H20,H2}$	$x_{N2,Ar,He}$	d_0 (mm)	$d(t_b)^*$ or d_{sat} (mm)	t_b^* or t_{sat} (s)	T_d (K)	$P_{Al.s}$ (atm)	C/C_{sat}	k_P (mm/s/atm CO)		
									n=2	n=1.5	n=1
0.4*	0.2	0.4	3.34	1.88	8.1	2450	0.17	0.89	0.063	0.065	0.068
0.4	0.2	0.4	3.25	1.8	8.4	2450	0.17	1.00	0.066	0.069	0.072
0.5*	0.5	0	3.41	1.56	5.1	2550	0.30	0.86	0.05	0.052	0.056
0.5*	Wet	0.5	3.12	1.96	8.9	2550	0.30	0.97	0.082	0.084	0.087
0.5	Wet	0.5	2.7	1.75	9.2	2550	0.30	1.00	0.079	0.081	0.084
0.8*	0.2	0	2.81	1.62	4.14	2600	0.39	1.00	0.09	0.093	0.097
0.8	0.2	0	3.17	1.68	5.25	2600	0.39	1.00	0.061	0.064	0.067
0.8	0.2	0	3.05	1.74	4.8	2600	0.39	1.00	0.081	0.084	0.088
0.8	0.2	0	3.26	1.7	5.36	2600	0.39	1.00	0.058	0.061	0.064
0.8	0.2	0	3	1.74	4.6	2600	0.39	1.00	0.088	0.091	0.095
0.8	0.2	0	3.15	1.88	4.8	2600	0.39	1.00	0.097	0.1	0.105
0.8	0.2	0	2.9	1.7	4.3	2600	0.39	1.00	0.094	0.098	0.102
0.8	0.2	0	3.31	1.86	4.9	2600	0.39	1.00	0.082	0.085	0.089
0.8	0.2	0	3.42	1.73	5.85	2600	0.39	1.00	0.051	0.053	0.056
0.875	0.125	0	3.22	1.97	4.65	2600	0.39	1.00	0.101	0.104	0.109
0.875	0.125	0	3.5	2.01	5.45	2600	0.39	1.00	0.077	0.08	0.083
1	Wet	0	3.31	1.78	6	2600	0.39	1.00	0.047	0.048	0.051
1	Wet	0	3.15	1.93	5.2	2600	0.39	1.00	0.078	0.081	0.084
1	0	0	3.4	2.41	3.5	2600	0.39	1.00	0.207	0.214	0.217
1	0	0	3.09	2.33	3.05	2600	0.39	1.00	0.27	0.275	0.28
1	0	0	3.15	2.38	3.35	2600	0.39	1.00	0.254	0.26	0.263
1	0	0	4.06	3.18	4.36	2600	0.39	1.00	0.29	0.295	0.3
1	0	0	2.5	1.7	2.7	2600	0.39	1.00	0.17	0.174	0.18
1	0	0	2.56	1.87	2.63	2600	0.39	1.00	0.23	0.234	0.24
1	0	0	3.2	2.25	3.86	2600	0.39	1.00	0.17	0.175	0.18
0.79	0	0.21He	3.28	2.49	3.84	2600	0.39	1.00	0.3	0.314	0.31
0.79	0	0.21He	3.5	2.65	3.89	2600	0.39	1.00	0.31	0.315	0.32
0.95	0.05 H_2	0	3.35	2.05	5.2	2600	0.39	1.00	0.087	0.09	0.093
0.88	0	0.12 Ar	3.33	2.52	4	2600	0.39	1.00	0.26	0.275	0.27
0.81	0	0.19 N_2	3.3	2.46	4.5	2600	0.39	1.00	0.23	0.234	0.24

Table 2 : Averaged values of both modes of k_P.

	d^2 law	$d^{1.5}$ law	d law
k_{P1} (mm/s/atm CO)	0.075±0.017	0.078±0.017	0.081±0.017
k_{P2} (mm/s/atm CO)	0.24±0.04	0.25±0.05	0.255±0.05

Table 3: Estimated values of $b°$ and e_{H2} for different activation energies, and droplet regression.

	d law		d^2 law	
E_a (eV)	$b°$	e_{H2}	$b°$	e_{H2}
0	0.0034±0.0003	0.31±0.03	0.0030±0.0003	0.30±0.03
0.5	0.031±0.003	0.31±0.03	0.028±0.003	0.31±0.03
1	0.29±0.03	0.32±0.03	0.26±0.03	0.32±0.03
1.27	1.0±0.1	0.32±0.03	-	-
1.3	-	-	1.0±0.1	0.32±0.03

Table 4: Extrapolated values of the carbon dissolution rate (k) with a d law for different activation energies, particle temperatures, and considering the influence of the hydrogenated species.

E_a (eV)	k (mm/s)	
	T=3000 K	T=3500 K
0	0.69	0.22
0.5	0.93	0.39
1	1.30	0.71
1.27	1.41	0.92

Table 5: Extrapolated values of the carbon dissolution rate (k) with a d^2 law for different activation energies, particle temperatures, and considering the influence of the hydrogenated species.

E_a (eV)	k (mm/s)	
	T=3000 K	T=3500 K
0	0.60	0.19
0.5	0.83	0.35
1	1.14	0.63
1.3	1.39	0.90

Table 6: Extrapolated range of a_1 values for the burning rate range β=5-30 mm/s (d_0<100 µm) and for different particle temperatures, and their corresponding range of d_{sat}/d_0, t_{sat}/t_b values.

T (K)	a_1	d_{sat}/d_0	t_{sat}/t_b
3000	1.8-22	0.64-0.34	0.36-0.66
3500	2.7-69	0.59-0.24	0.41-0.76

Table 7: Extrapolated range of a_2 values for the burning rate range β=0.2-0.5 mm²/s and for different particle temperatures and sizes, and their corresponding range of d_{sat}/d_0, t_{sat}/t_b.

T (K)	a_2		d_{sat}/d_0		t_{sat}/t_b	
	30 µm	120 µm	30 µm	120 µm	30 µm	120 µm
3000	0.40-2.30	0.10-0.58	0.68-0.44	0.83-0.62	0.57-0.75	0.41-0.62
3500	0.63-7.33	0.16-1.83	0.62-0.32	0.78-0.47	0.62-0.82	0.47-0.73

Figure captions

Figure 1: Carbon ejection process and interaction with the oxide cap at the surface of an aluminum droplet burning in 100% CO_2.

Figure 2: Carbon dissolution kinetics for an aluminum droplet (d_0=3 mm) considering a d^2 law (β_2=1.5 mm^2/s), and for different carbon dissolution rates.

Figure 3: Simulation of the carbon dissolution kinetics for an aluminum burning droplet for three regression laws based on experimental data. x_{CO2}=0.8, d_0=3.05 mm, d_{sat}=1.74 mm, t_{sat}=4.8 s, T_d=2600 K.

Figure 4: Distribution of k_P (step 0.02 from 0 to 0.15; step 0.04 from 0.15 to 0.35).

Figure 5: CO and Al vapor pressures at the particle surface as a function of the temperature with P_T=60 atm, and $x_{CO,f}$=0.3.

Figure 6: Variation of d_{sat}/d_0 and t_{sat}/t_b as a function of parameter $a_1=\beta/2k$ for a "d law". ○: experimental data. Dotted zone: extrapolation range.

Figure 7: Variation of d_{sat}/d_0 as a function of parameter $a_2=\beta/(12k \cdot d_0)$ for different initial diameters and considering a "d^2 law". ○: experimental data. Extrapolation ranges: zone \\ for d_0=30 µm, and zone // for d_0=120 µm.

Figures

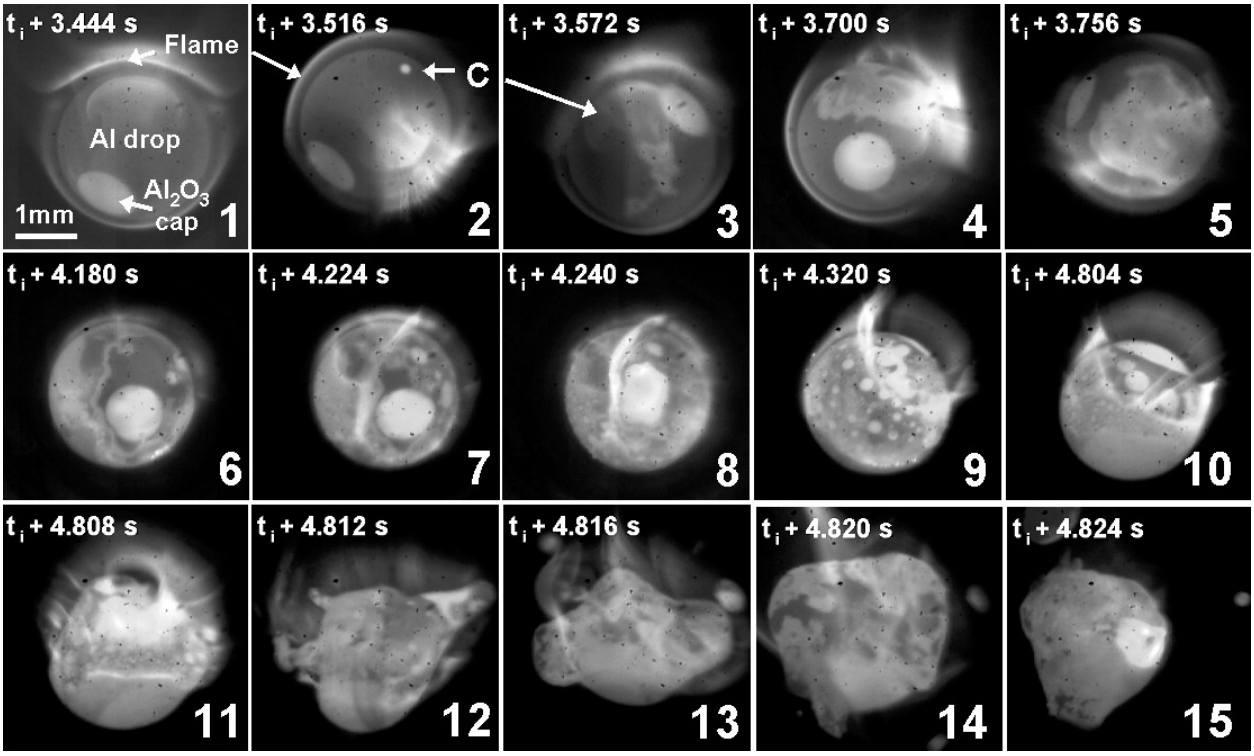

Figure 1

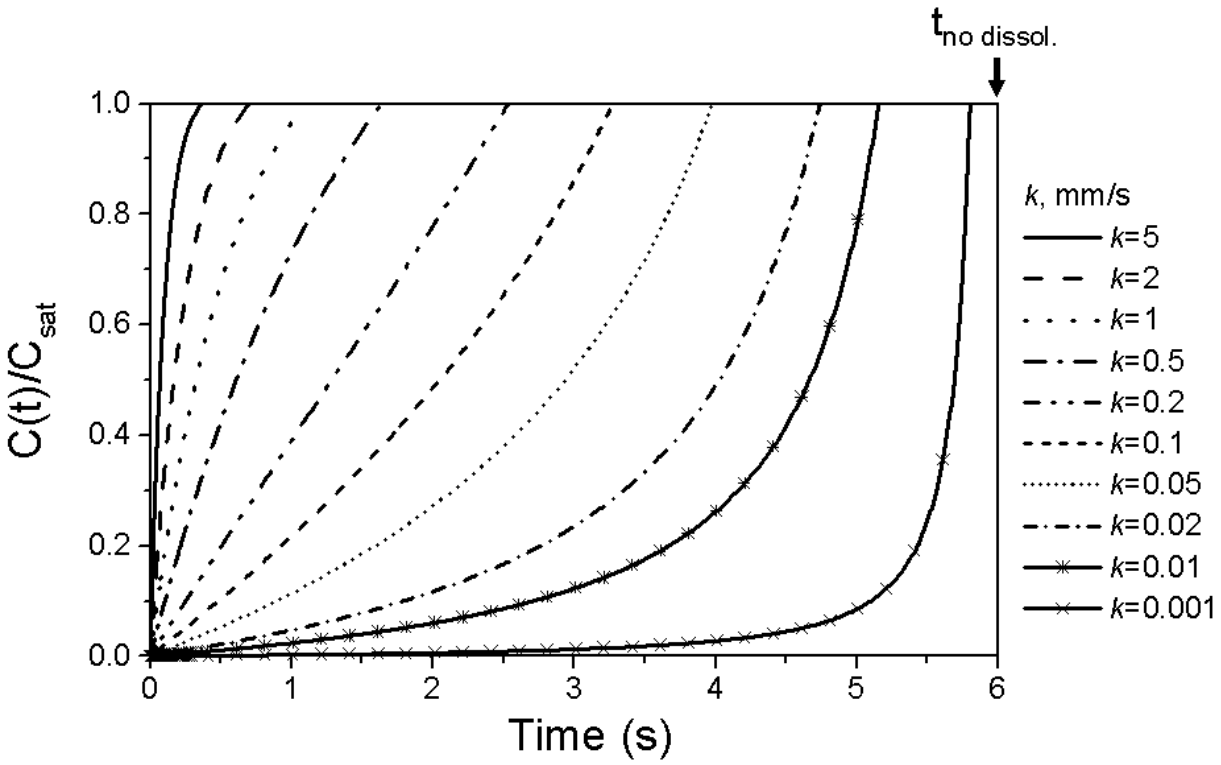
t no dissol.
1.0
0.8
0.6
0.4
0.2
0.0
C(t)/C sat
0
1
2
3
4
5
6
Time (s)
k, mm/s
k=5
k=2
k=1
k=0.5
k=0.2
k=0.1
k=0.05
k=0.02
k=0.01
k=0.001

Figure 2

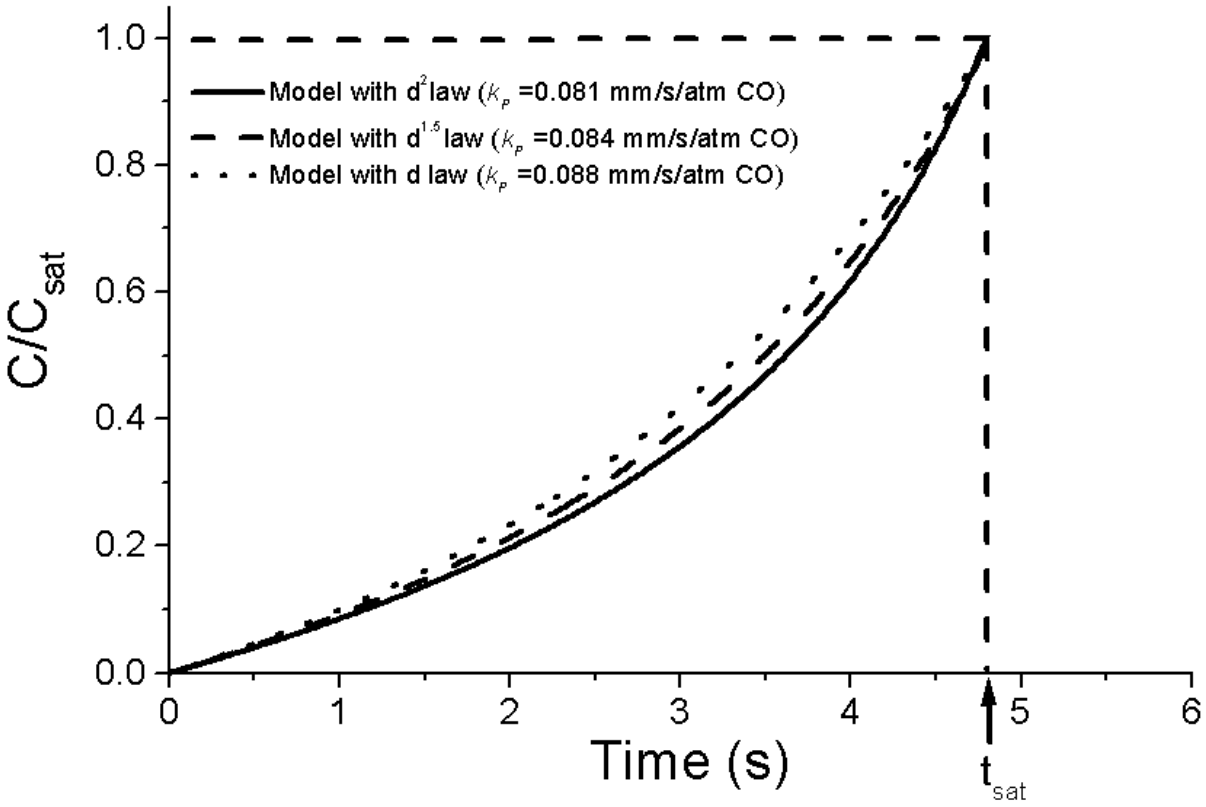
Model with d^2 law (k_p =0.081 mm/s/atm CO)
Model with d^1.5 law (k_p =0.084 mm/s/atm CO)
Model with d law (k_p =0.088 mm/s/atm CO)
C/C_sat
Time (s)
t_sat
0.0
0.2
0.4
0.6
0.8
1.0
0
1
2
3
4
5
6

Figure 3

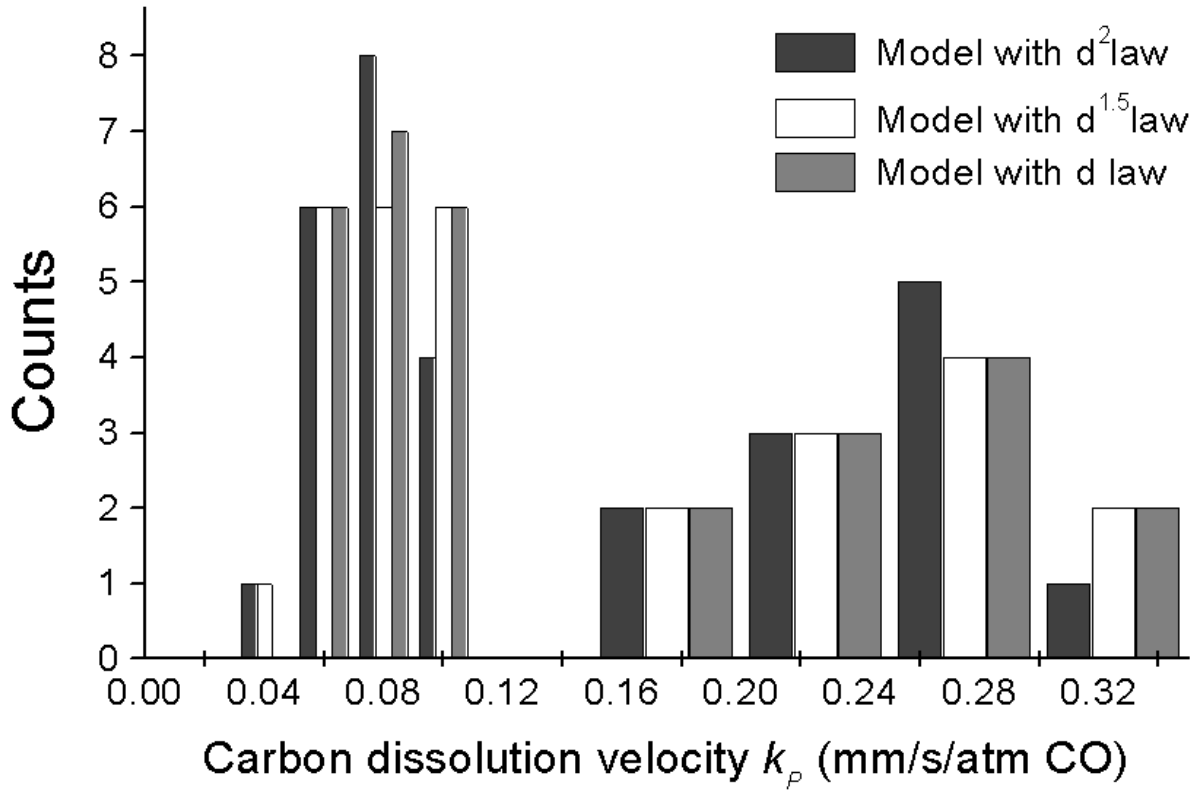
Model with d^2 law
Model with d^1.5 law
Model with d law
Counts
0
1
2
3
4
5
6
7
8
0.00
0.04
0.08
0.12
0.16
0.20
0.24
0.28
0.32
Carbon dissolution velocity k_P (mm/s/atm CO)

Figure 4

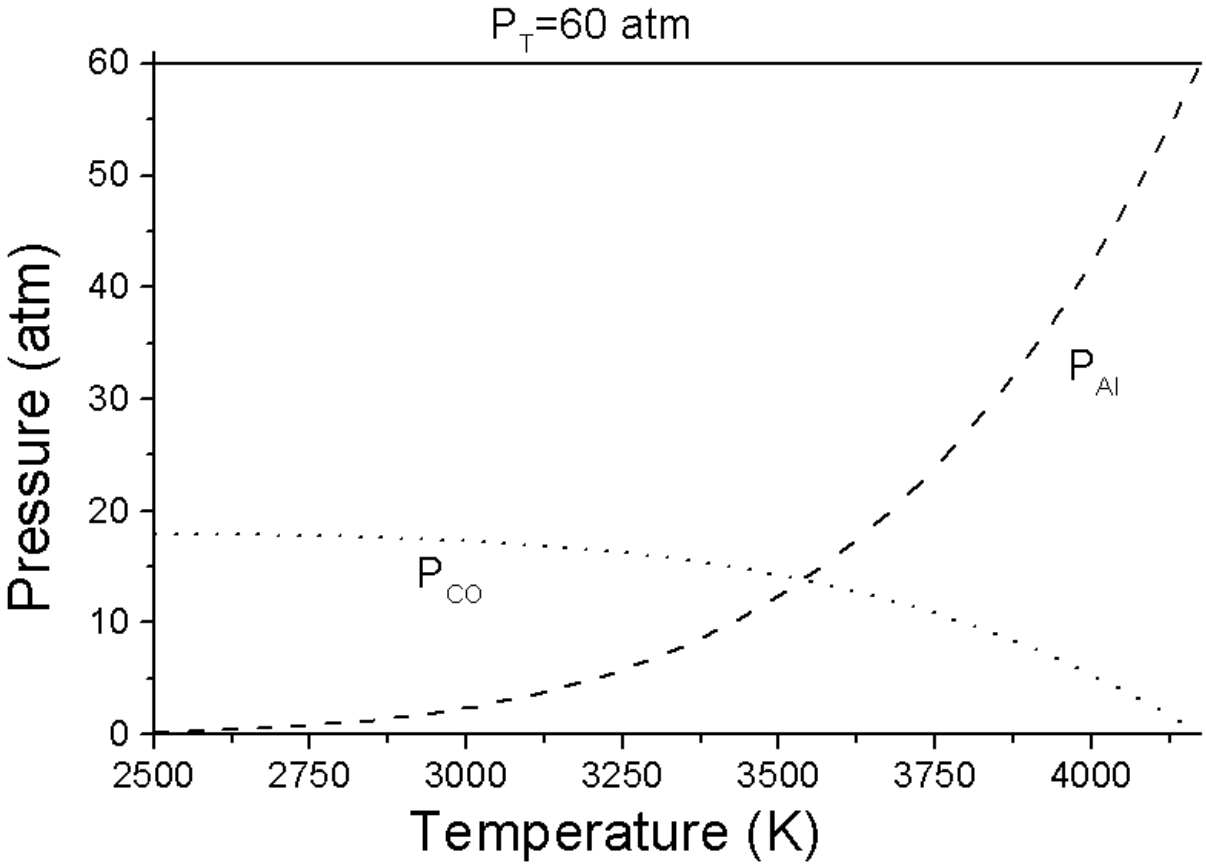
P_T=60 atm
Pressure (atm)
Temperature (K)
P_CO
P_Al
0
10
20
30
40
50
60
2500
2750
3000
3250
3500
3750
4000

Figure 5

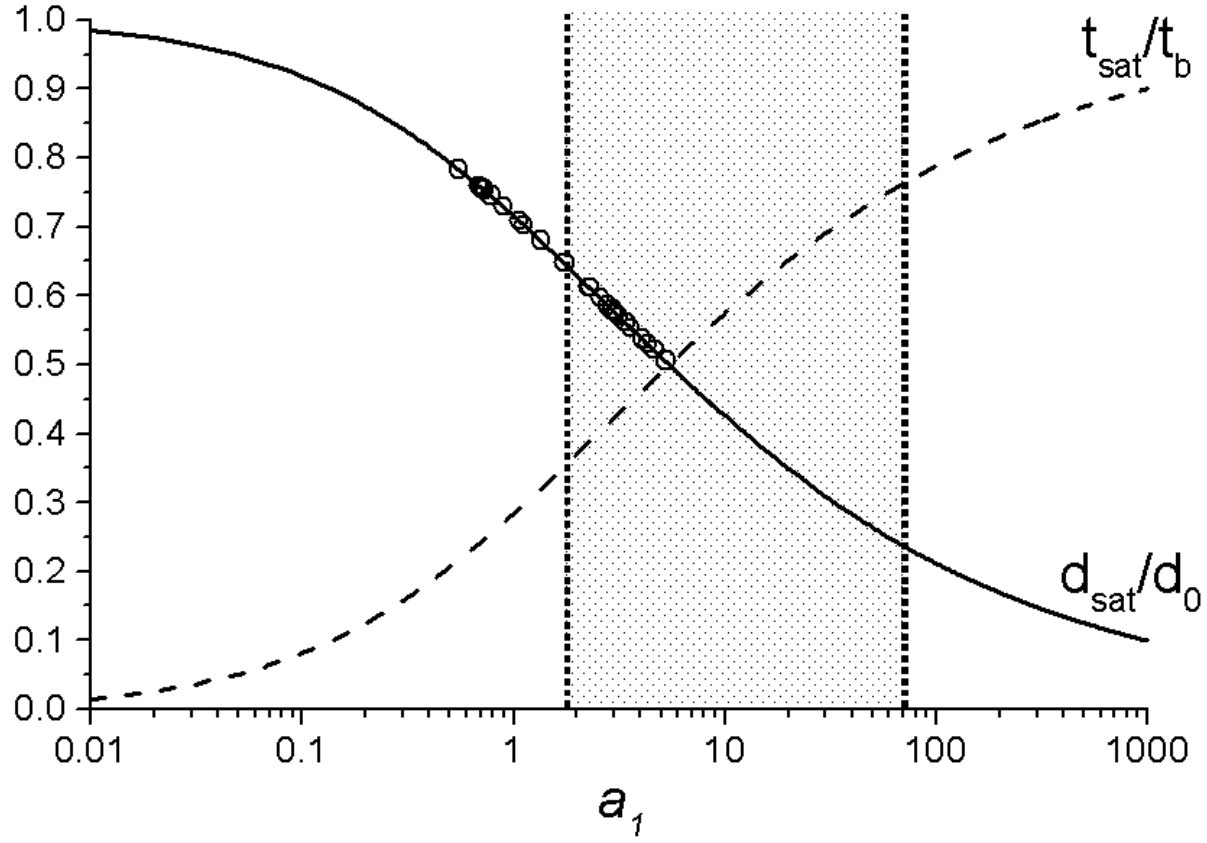
1.0
0.9
0.8
0.7
0.6
0.5
0.4
0.3
0.2
0.1
0.0
0.01
0.1
1
10
100
1000
a_1
t_{sat}/t_b
d_{sat}/d_0

Figure 6

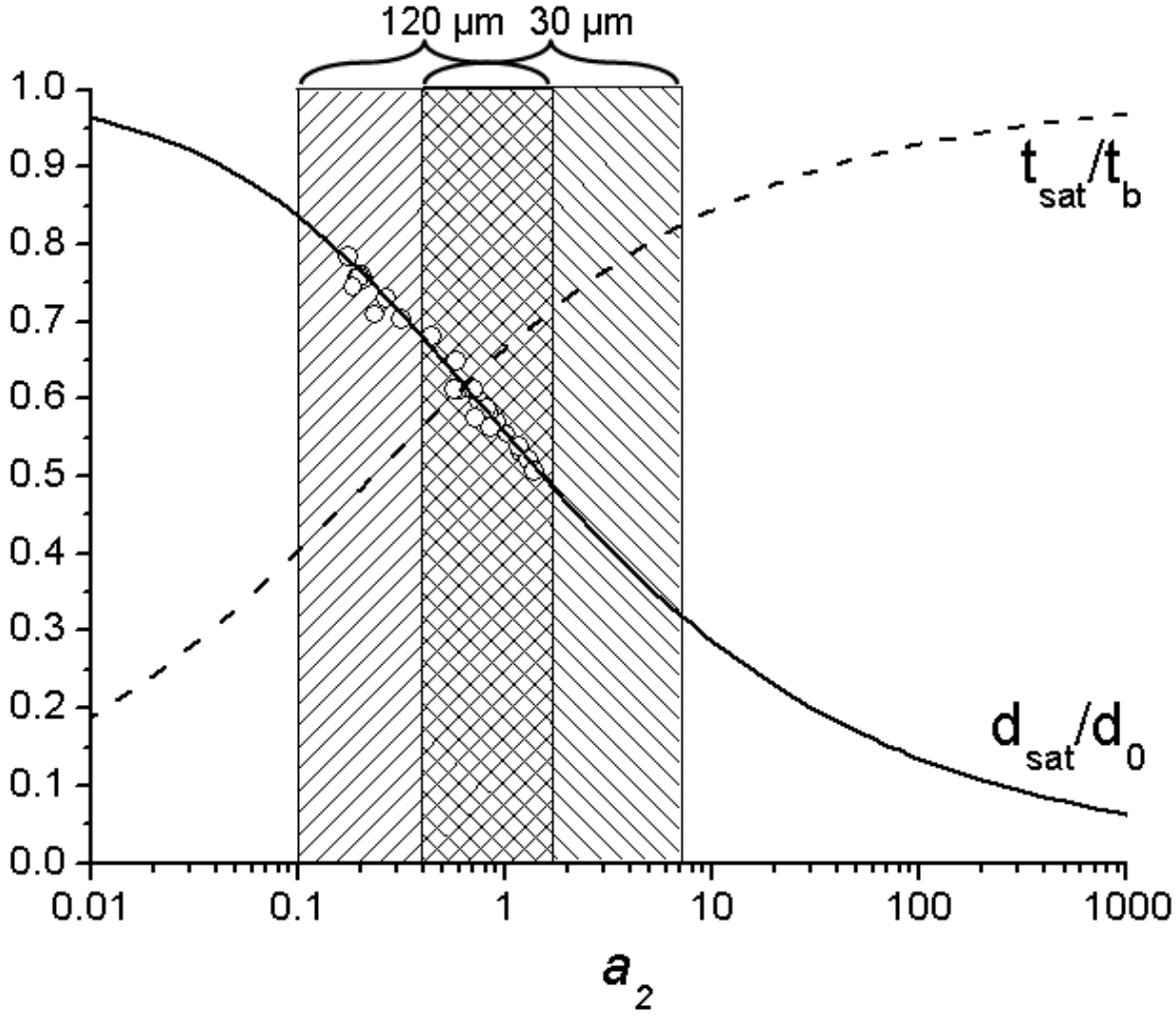
120 µm
30 µm
1.0
0.9
0.8
0.7
0.6
0.5
0.4
0.3
0.2
0.1
0.0
0.01
0.1
1
10
100
1000
a2
tsat/tb
dsat/d0

Figure 7